Optical Materials 32 (2010) 1385–1388

Contents lists available at ScienceDirect

Optical Materials

journal homepage: www.elsevier.com/locate/optmat

Crystallization effect on Tm^{3+}–Yb^{3+} codoped SBN glass ceramics

P. Haro-González [a,*], I.R. Martín [a,1], L.L. Martín [a], D. Kowalska [a], J.M. Cáceres [b]

[a] Departamento de Física Fundamental, Experimental, Electrónica y Sistemas, Universidad de La Laguna, 38206 La Laguna, Tenerife, Spain
[b] Departamento de Edafología y Geología, Universidad de La Laguna, 38206 La Laguna, Tenerife, Spain

ARTICLE INFO

Article history:
Received 3 November 2009
Accepted 3 May 2010
Available online 28 April 2010

Keywords:
Er^{3+}
Glass ceramics
SBN
Optical materials
Laser spectroscopy
Rare-earth

ABSTRACT

An appropriated thermal treatment of SrO–BaO–Nb_2O_5–B_2O_5 glass leads to the formation of glass ceramics which are composed of Tm^{3+}–Yb^{3+} codoped strontium barium niobate (SBN) nanocrystals dispersed throughout an amorphous matrix. The glasses have been fabricated using a melt-quenching method and after a thermal treatment at 620 °C have been obtained the glass ceramic samples. The formation of SBN nanocrystals has been confirmed by the X-ray diffraction patterns. Visible and NIR emission spectra have been reported and confirmed the incorporation of the Tm^{3+}–Yb^{3+} ions into the SBN nanocrystals. In the glass ceramics samples the decays of Tm^{3+} levels for the Yb^{3+}–Tm^{3+} codoped samples are longer than in the Tm^{3+} single doped samples. This surprising result could be explained in basis to the localisation of the active ions in the SBN nanocrystals.

1. Introduction

Strontium barium niobate $Sr_xB_{a1-x}Nb_2O_6$ (SBN) belongs to the ferroelectric crystals family with interesting dielectric, nonlinear optic and electro-optic properties [1]. This photorefractive material has several potential applications like electro-optic modulation, holographic data storage, pyroelectric detection and surface acoustic wave devices [2–5].

Doping of SBN crystals with rare-earth [RE] ions can modify its physical properties and the luminescence can be quenched or enhanced due to energy transfer processes [6–10]. Weakly coupled electronic levels to the lattice vibrations in these ions are responsible for the sharp line spectra. On the another hand the Yb^{3+}–Tm^{3+} system has been studied due to its conversion an infrared radiation into visible light [11–13].

In this paper we will present spectral and photophysical properties of Tm^{3+}–Yb^{3+} codoped glass matrixes in glassy and nanocrystalline phases. The strontium barium niobate glasses codoped with Yb^{3+} and Tm^{3+} ions have been prepared by melt-quenching method. The presence of nanocrystals with an average diameter around 50 nm in the glass ceramic matrix was confirmed by the X-ray diffraction measurements [14]. The decay curves from the $^1G_4$, $^3H_4$ and $^2F_{5/2}$ levels have been analyzed in the glass and glass ceramics samples.

2. Experimental

The samples were prepared using the melt-quenching method with the following composition x Tm_2O_3, y Yb_2O_3, 11.25 SrO, 11.25 BaO, 22.5 Nb_2O_5, and $(55 - x - y)$ B_2O_3 in mol% with x and y equal to 0 or 1. Commercial powders of reagent grade were mixed and melted in platinum crucible at 1400 °C inside an electric furnace during 1 h. The melted mixture was poured between two iron plates with the distance of 1.6 mm between them. The glass precursor was heated in isothermal condition at 620 °C for 4 h in an electric furnace to form the glass ceramic sample. Different thermal treatments have been carried out to the samples (2, 3 or 4 h) in order to check the formation of the nanocrystals. All the spectroscopic experiments were carried out for the sample with 4 h of thermal treatment. The sample surface was polished in order to reduce laser light divergence during excitation.

X-ray diffraction was carried out with a diffractometer (Panalytical ẊPert) using a Cu K_α radiation as a source. The continuous wave Ar-laser with excitation wavelength 488 nm was used for stationary emission measurements from the $^1G_4$, $^3H_4$, $^2F_{5/2}$ levels. The measurements were carried out with an Ocean-Optic High Resolution Spectrometer. The emission decay measurements were obtained using an OPO laser with excitation wavelengths at 475, 800 and 920 nm. Digital oscilloscope LeCroy Wave Surfer 424 was used as a detection system. The upconversion emission spectra were obtained under a continuous diode laser at 950 nm.

* Corresponding author.
E-mail address: patharo@ull.es (P. Haro-González).
[1] MALTA Consolider Team.

0925-3467/$ - see front matter © 2010 Elsevier B.V. All rights reserved.
doi:10.1016/j.optmat.2010.03.014

3. Results and discussion

The X-ray diffraction (XRD) spectra of the glass and glass ceramic samples codoped with 1.0 mol% of Yb^{3+} and 1.0 mol% of Tm^{3+} are shown in Fig. 1. According to these data, the glass sample is X-ray amorphous with a broad diffraction curve. The thermal treatment for the initial glass was carried out in an isothermal condition at 620 °C during 2–4 h. With increasing the heat treatment time, the characteristic narrow peaks attributed to the SBN crystalline phase started to appear. The amount of the peaks and their intensity are increasing with the time of thermal treatment. The SBN nanosized crystals were formed in the material with diameter around 50 nm estimated from the Scherreŕs formula [14]. All the spectroscopic experiments were carried out for the sample with 4 h of thermal treatment.

The schematic energy-level diagram of Yb^{3+} and Tm^{3+} ions has been shown in Fig. 2 in which are sketched only the levels interested for the study in the present work. The continuous wave Ar: laser with the excitation wavelength at 488 nm populated the $^1G_4$ level in the glass and glass ceramic samples. The fluorescence

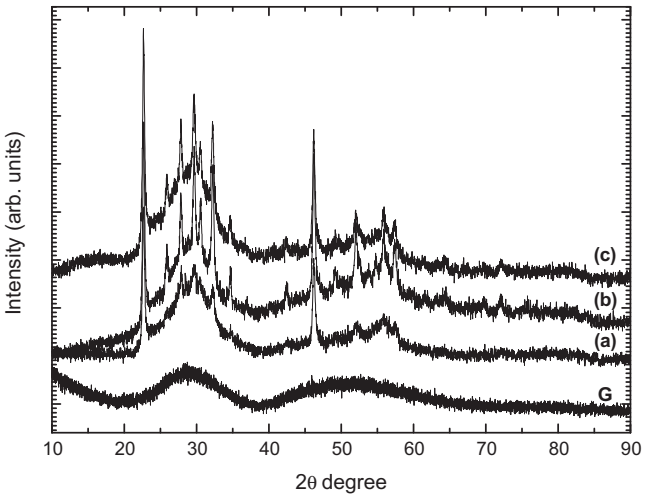

Fig. 1. XRD patterns of the glass (G) and glass precursor samples as function of the thermal treatment for (a) 2 h, (b) 3 h, and (c) 4 h.

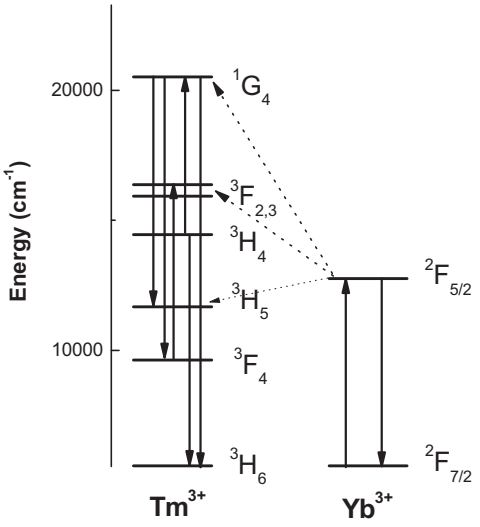

Fig. 2. Energy-level diagram of Tm^{3+} and Yb^{3+} ions and upconversion mechanism under excitation the Yb^{3+} ions.

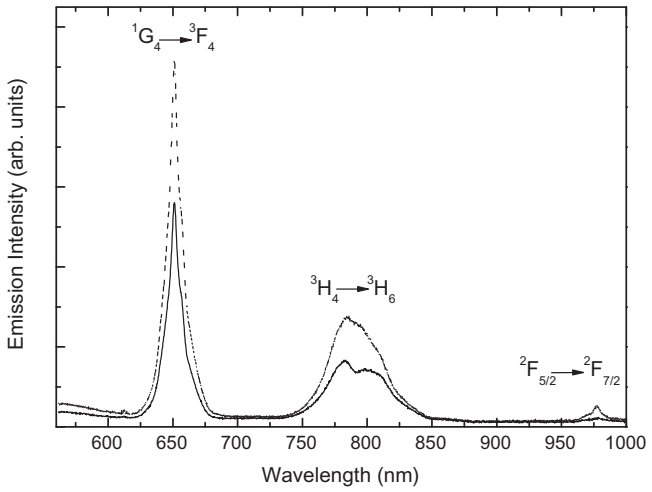

Fig. 3. Fluorescence emission spectra of Tm^{3+}–Yb^{3+} codoped samples for the glass (—) and glass ceramic (- - -) samples under excitation at 488 nm.

visible and IR emissions were observed at room temperature for Tm^{3+}–Yb^{3+} codoped glass and glass ceramic samples (Fig. 3). The red emission band is assigned to the Tm^{3+} transition $^1G_4 \rightarrow {}^3F_4$ and the IR emission bands are assigned to transitions $^3H_4 \rightarrow {}^3H_6$ and $^2F_{5/2} \rightarrow {}^2F_{7/2}$ of Tm^{3+} and Yb^{3+} ions, respectively. Changes in the shape of fluorescence emission spectra for glass ceramic sample compared to glass sample are observed for $^3H_4 \rightarrow {}^3H_6$ transition. Moreover for the glass ceramic sample appeared the second IR band corresponded to the $^2F_{5/2} \rightarrow {}^2F_{7/2}$ transition of Yb^{3+} ions.

The fluorescence decay curves for the $^2F_{5/2} \rightarrow {}^2F_{7/2}$ level obtained for the glass and glass ceramic samples single doped with 1% mol Yb^{3+} and codoped with 1% mol Yb^{3+} and 1% mol Tm^{3+} are presented in Fig. 4. The emission lifetimes for glass and glass ceramic samples single doped with Yb^{3+} ions are significantly longer than emission lifetimes for codoped glass and glass ceramic samples. It shows that an energy transfer process between these two ions plays an important role in the quenching of the emission lifetime of $^2F_{5/2}$ level of Yb^{3+} ions. This energy transfer process is given by the well known channel [15]:

$$^2F_{5/2}\,(Yb^{3+}),\ {}^3H_6(Tm^{3+}) \rightarrow {}^2F_{7/2}\,(Yb^{3+}),\ {}^3H_5(Tm^{3+}).$$

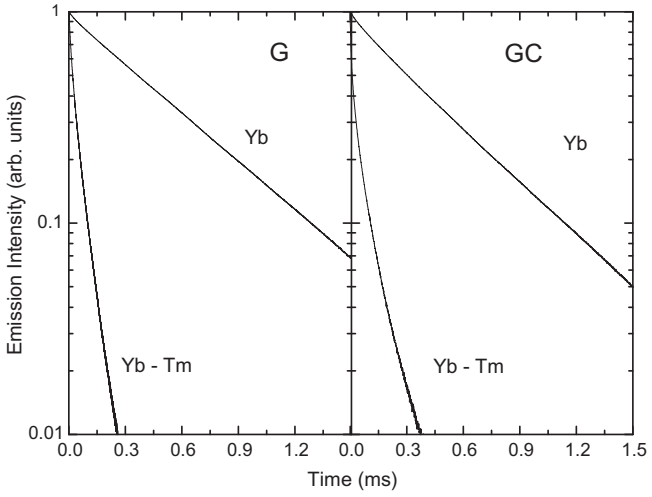

Fig. 4. Emission decay curves for the $^2F_{5/2} \rightarrow {}^2F_{7/2}$ level obtained for the glass (G) and glass ceramic (GC) samples doped with 1 mol% of Yb^{3+} ions and codoped with 1 mol% of Yb^{3+} and 1 mol% of Tm^{3+} ions under excitation at 920 nm.

This process is a nonresonant energy transfer process and it needs the emission of several phonons to the matrix. According to the experimental decays, this process is more efficient for glass sample than the glass ceramic sample. This result could be explained in basis to the higher phonons in the oxide glass matrix [4].

A different behaviour is obtained for the fluorescence decay curves for the $^3H_4$ level obtained for the same doped glass and glass ceramics samples (see Fig. 5). As it is expected, when the glass samples are codoped with Yb^{3+} ions, the lifetime of the $^3H_4$ level decreases due to an energy transfer between these two ions. This process could be explained due to the following energy transfer channel:

$$^3H_4\ (Tm^{3+}),\ ^2F_{7/2}\ (Yb^{3+}) \rightarrow {}^3H_6\ (Tm^{3+}),\ ^2F_{5/2}\ (Yb^{3+}).$$

This mechanism is a nonresonant energy transfer process and requires the participation of phonons. Respect to the glass ceramic sample, it must be taken into account that it contains glassy and nanocrystalline phases. Therefore, the initial part of the emission decay is assigned to the glassy phase, and the long component to the emission of the ions which reside into the nanocrystals. However, it is interesting to note that in the codoped sample the decay is slightly slower than in the single doped sample.

This previous result is surprising and in order to obtain an explanation the decay curves for the $^1G_4$ level have been also measured. Therefore, in Fig. 6 the decay curves for this level are shown. In this figure, as it is expected, the decay curve for the glass sample is faster when the sample is codoped with Yb^{3+} ions. This energy transfer process could be due to the following energy transfer channel:

$$^1G_4\ (Tm^{3+}),\ ^2F_{7/2}\ (Yb^{3+}) \rightarrow {}^3H_5\ (Tm^{3+}),{}^2F_{5/2}\ (Yb^{3+}).$$

With regard to the glass ceramics samples, as it is shown in Fig. 6, the decay curve for the codoped sample is a little bit slower than the for the single doped sample. This surprising behaviour is exactly the same that it has been found for the decays shown in Fig. 5.

In order to explain this not usual behaviour in the energy transfer processes the projection of the SBN structure to the *c-plane* [9,16] is shown in Fig. 7. Considering the ionic radii of Ba^{2+} (0.136 nm), Sr^{2+} (0.113 nm) and RE^{3+} (~0.10 nm), rare-earth ions might be mainly substituted at the site of Sr^{2+} in SBN crystals [9,16] as it is shown in this figure. In codoped nanocrystals the

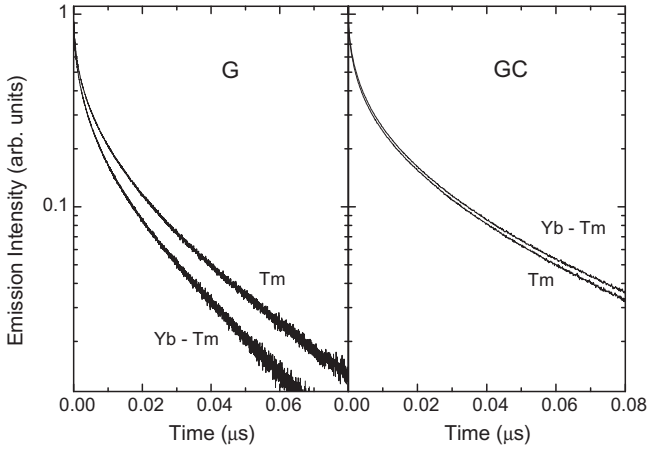

Fig. 6. Emission decay curves for the $^1G_4$ level obtained for the glass (G) and glass ceramic (GC) samples doped with 1 mol% of Yb^{3+} ions and codoped with 1 mol% of Yb^{3+} and 1 mol% of Tm^{3+} ions under excitation at 475 nm.

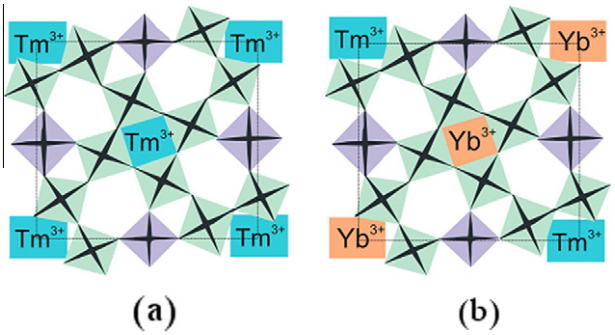

Fig. 7. Representation of the unit cell of SBN crystal doped with Tm^{3+} ions (a) and codoped with Tm^{3+}–Yb^{3+} ions (b).

Yb^{3+} ions could be located in intermediate positions between Tm^{3+} ions. In this situation the average distance between the Tm^{3+} ions is increasing and the cross relaxation processes between these ions are decreasing. Therefore, the surprising behaviour obtained in Figs. 5 and 6, where the decay curves are longer in codoped samples, is due to a decreasing of the cross relaxation processes between these ions [17]. However, the decay curves

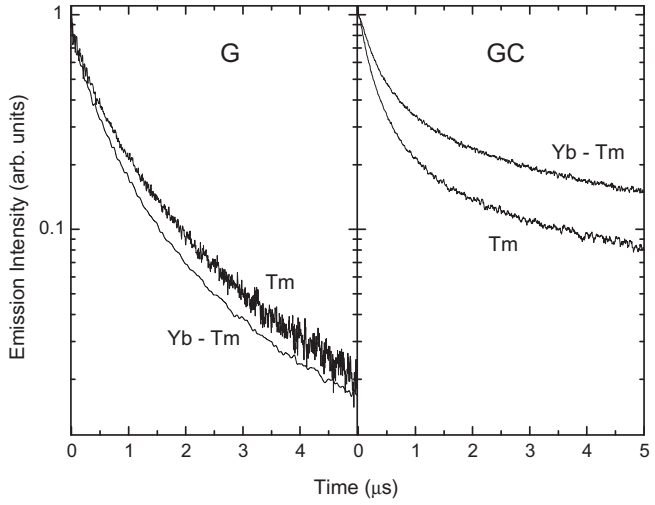

Fig. 5. Emission decay curves for the $^3H_4$ level obtained for the glass (G) and glass ceramic (GC) samples doped with 1 mol% of Yb^{3+} ions and codoped with 1 mol% of Yb^{3+} and 1 mol% of Tm^{3+} ions under excitation at 800 nm.

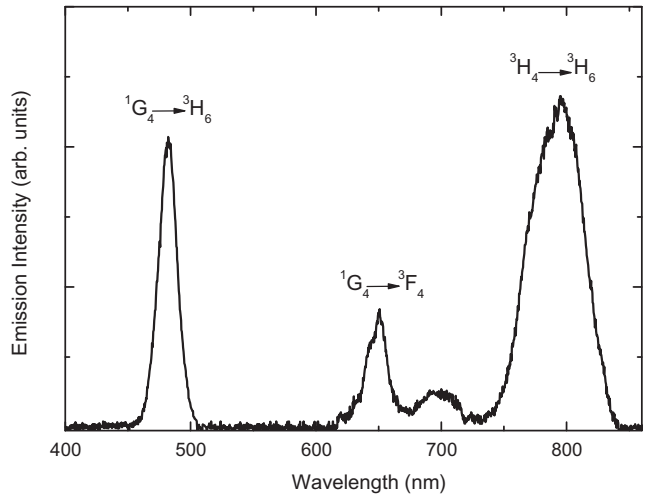

Fig. 8. Upconversion emission spectrum by exciting at 950 nm in Tm^{3+}–Yb^{3+} codoped glass ceramic sample.

obtained for Yb^{3+} ions (Fig. 4) do not show this effect because these ions have not cross relaxation processes among them.

Finally in Fig. 8 is presented the upconversion spectrum under excitation at 950 nm (Yb^{3+}: $^2F_{7/2} \rightarrow {}^2F_{5/2}$) for glass ceramic codoped sample. The upconversion emission bands centred at 482, 650 and 795 nm are attributed to the transitions $^1G_4 \rightarrow {}^3H_6$, $^1G_4 \rightarrow {}^3F_4$ and $^3H_4 \rightarrow {}^3H_6$, respectively. It is interesting to note that for the glass samples negligible upconversion emissions are detected. This result could be explained in basis to the main role of the intermediate levels in this upconversion process ($^3H_4$ and $^3F_4$ levels) schematized in Fig 2. As example, the long component of the decay curve for the $^3H_4$ level is assigned to ions which reside into the nanocrystals (see Fig. 5). Therefore, this long metastable level plays a main role in order to obtain efficient blue upconversion emission as it is indicated in Fig. 2.

4. Conclusions

Strontium barium niobate glasses have been doped with Tm^{3+} and codoped with Tm^{3+}–Yb^{3+} ions. In these samples after a thermal treatment at 620 °C have started to growth SBN nanocrystals with an average size of 50 nm. The emission spectra and the decay curves show that the active ions are incorporated into these nanocrystals. The analysis of the decays curves indicates a non-usual behaviour for the decay curves of the Tm^{3+} ions in the nanocrystals. The codoped glass ceramics samples with Yb^{3+} ions have longer decays than the single doped with Tm^{3+} ions. This result could be explained in basis to the incorporation of the active ions into the SBN nanocrystals. Finally, the upconversion processes under excitation at 950 nm are very efficient in the glass ceramics samples whereas are negligible in the glass samples. This result could be explained by the long lifetime of the levels involved in the upconversion mechanism and it is the object of a future research.

Acknowledgements

The authors gratefully acknowledge the financial support of this research by the Comisión Interministerial de Ciencia y Tecnología (MAT-2007-63319 and MAT-2007-65990-C03-02), Malta Consolider-Ingenio 2010 (CSD2007-0045) and FPI grant by Agencia Canaria de Investigación del Gobierno de Canarias.

References

[1] A.M. Glass, J. Appl. Phys. 40 (1969) 4699.
[2] H. Liu, S.T. Li, F.E. Fernandez, G.K. Liu, Thin Solid Films 424 (2003) 61–65.
[3] T. Volk, D. Isakov, V. Salobutin, L. Ivleva, P. Lykov, V. Ramzaev, M. Wöhlecke, Solid State Commun. 130 (2004) 223–226.
[4] N. Chayapiwut, T. Honma, Y. Benino, T. Fujiwara, T. Komatsu, J. Solid State Chem. 178 (2005) 3507–3513.
[5] T.P.J. Han, F. Jaque, D. Jaque, J. García-Sole, L. Ivleva, J. Lumin. 119–120 (2006) 453–456.
[6] K. Masuno, J. Phys. Soc. Jpn. 19 (1964) 323.
[7] N. Wakiya, J.K. Wang, A. Saiki, K. Shinozaki, N. Mizutani, J. Eur. Ceram. Soc. 19 (1999) 1071.
[8] J.J. Romero, D. Jaque, L.E. Bausá, A.A. Kaminskii, J. García Solé, J. Lumin. 87–89 (2000) 877–879.
[9] W. Sakamoto, M. Mizuno, T. Yamaguchi, K. Kikuta, S. Hirano, Jpn. J. Appl. Phys. 42 (2003) 5913.
[10] P. Haro-González, F. Lahoz, J. González-Platas, J.M. Cáceres, S. González-Pérez, D. Marrero-López, N. Capuj, I.R. Martín, J. Lumin. 128 (2008) 908–910.
[11] I.R. Martín, V.D. Rodríguez, V. Lavín, U.R. Rodríguez-Mendoza, Spectrochim. Acta Part A 55 (1999) 941–945.
[12] Wenwei Xu, Xiaodong Xu, Feng Wu, Guangjun Zhao, Zhiwei Zhao, Guoqing Zhou, Jun Xu, Opt. Commun. 272 (2007) 182–185.
[13] P. Haro-González, I.R. Martín, S. González-Pérez, M. Liu, S.W. Wang, N. Capuj, F. Lahoz, J. Lumin. 128 (2008) 924–926.
[14] P. Klug, L.E. Alexander, X-ray Diffraction Procedure, Wiley, New York, 1954 (Chapter 9).
[15] J. Méndez-Ramos, F. Lahoz, I.R. Martín, A.B. Soria, A.D. Lozano-Gorrín, V.D. Rodríguez, Mol. Phys. 101 (2003) 1057.
[16] N. Chayapiwut, T. Honma, Y. Benino, T. Fujiwara, T. Komatsu, Solid State Chem. 178 (2005) 3507.
[17] I.R. Martín, V.D. Rodríguez, R. Alcalá, R. Cases, J. Non-Cryst. Solids 161 (1993) 294.